TECHNICAL REPORT

SPACE TELESCOPE SCIENCE INSTITUTE
Operated for NASA by AURA

Title: Self –Calibration and the Dither Patterns for NIRCam and MIRI	Doc #: JWST-STScI-001950, SM-12 Date: January 26, 2009 Rev: -
Authors: Jay Anderson & Christine Chen Phone:*410-338-4982*	Release Date: 18 March 2010

1.0 ABSTRACT

NIRCam and MIRI have recently put together sets of imaging dither patterns that have been optimized for the anticipated science goals of each instrument. The MIRI set contains patterns that are explicitly optimized for self-calibration, whereas the NIRCam patterns are all optimized for sub-pixel resolution, L-flat mitigation, and gap coverage, without the explicit goal of self-calibration. A data set that is optimized for self-calibration is taken in such a way that the flat fields and/or the bias can be solved-for internally, without reference to formal calibration observations. There are circumstances where such a self-calibration can improve the final data quality. This document will describe why self-calibration is a relevant goal for MIRI, but not for NIRCam.

2.0 INTRODUCTION

NIRCam and MIRI have recently put together sets of dither patterns that have been optimized for the anticipated science goals of each instrument (see Anderson 2009 for the proposed NIRCam patterns and Chen 2009 for the proposed MIRI patterns). The question has come up informally as to why MIRI has patterns that are optimized for self-calibration, whereas NIRCam does not. This document is an effort to address that question.

We begin with a brief presentation of the dithering strategies devised for the two instruments. We will then give a brief description of the goals and requirements for self-calibration. Finally, we will discuss how the dither strategies for NIRCam and MIRI relate to self-calibration.

3.0 CURRENT NIRCam AND MIRI DITHER STRATEGIES

In this section we will give an overview of the dithering strategies devised for NIRCam and MIRI imaging. Both instruments have divided their dithering strategies into primary

and secondary dither patterns. The secondary dither patterns for both are designed to mitigate the effect of PSF-undersampling, which is non-existent to mild for MIRI and moderate to severe for NIRCam. The primary patterns of the two instruments are quite different, and this document is an effort to explain why. For the rest of the document, when we refer to dithering, we will be referring to the "primary" (larger-offset) dithers.

3.1 NIRCam dither strategy

NIRCam has three main primary dither patterns: (1) the full-field pattern, (2) the intra-module pattern, and (3) the intra-SCA pattern. The NIRCam footprint is shown in Figure 1. There is a large vertical gap of 40″ between the modules, and smaller vertical and horizontal gaps of 5″ between the SCAs (sensor-chip assemblies; the individual 2048×2048 detectors, of which there are 8 in the short-wave channel and 2 in the long-wave channel).

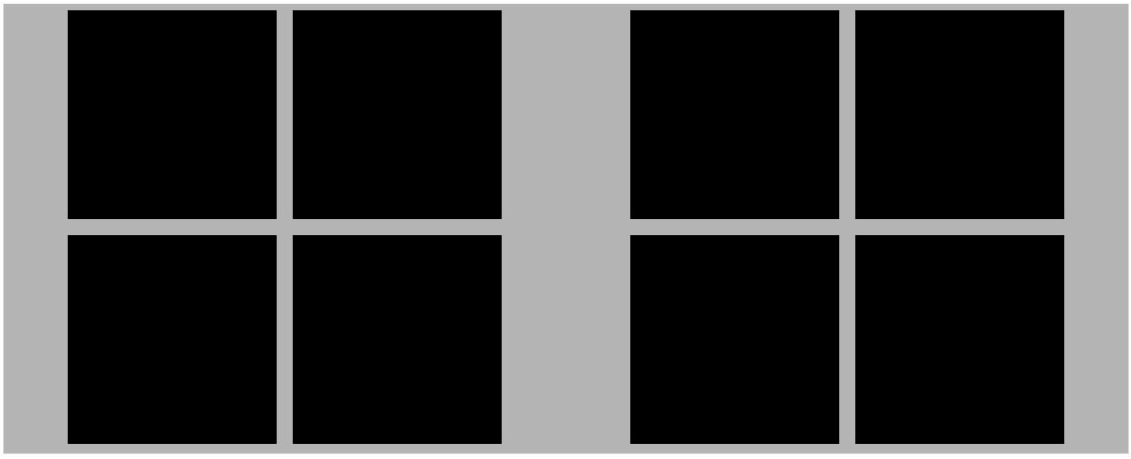

Figure 1: NIRCam footprint for the short-wave channel. There are two modules, and each module is made up of an array of 2×2 detectors. The module gap is about 40″ and the SCA gap is about 5″.

The main focus of the first two NIRCam patterns is to mitigate the effects of gaps in the footprint by ensuring that any given source will fall into the gaps a minimal number of times. The first pattern is designed to account for the effects of both the large and the small gaps, and the second pattern deals only with the small gaps between SCAs. In addition to minimizing the impact of the gaps, the patterns are also designed to place each source at a variety of locations within the footprint, which naturally averages down errors due to low-frequency flat-field ("L-flat") calibrations. The third pattern is designed to work within a single SCA, so it has no gaps to concern itself with; its main focus is to place the target at a variety of locations within the chip in order to randomize as much as possible any L-flat or other spatially dependent calibration errors.

In summary, there are two main focuses for the NIRCam dither strategy. The mitigation of field lost to the gaps, and the mitigation of L-flat-type errors. The two aims are complementary: we get both optimal gap mitigation and L-flat mitigation at the same time by moving the sources around within the FOV.

3.2 MIRI dither strategy

MIRI has two primary dither patterns: a 12-point Reuleaux pattern and a 311-point cycling pattern. Each pattern is available in three size-scales (small, medium, and large) that, by default, are automatically selected by APT for the user based on the observation wavelength. These patterns are drawn from the Spitzer IRAC dither patterns (Carey et al. 2010) that were optimized for self-calibration. The first pattern is designed to move a target around the perimeter of a rounded triangle, where the points have been chosen such that the offsets between the dithers are all unique. The second primary pattern is a 311-point cycling pattern, which has been chosen such that the dither offsets are distributed in a Gaussian way no matter where the pattern is started, and no matter how many steps of the pattern are executed.

The MIRI patterns were designed with two aims in mind. There are no gaps in the MIRI imaging field of view, so this main driver for NIRCam dithering was not a concern for MIRI. As with NIRCam, one of the MIRI dithering goals was to mitigate any flat-fielding errors that may be present in the pipeline reductions. For this reason, the dither offsets are always more than several PSF FWHMs, to ensure that each time a star is imaged, it will land on different pixels, so that any local flat-field errors would average out.

In addition to mitigating flat-fielding errors that may be present, the two MIRI patterns were also devised to allow deep data sets to perform a self-calibration. Such a supplementary calibration can be useful in the event where the pipeline calibrations are not sufficiently accurate, because of time variation either of the reference files or of the background. There are many considerations involved in self-calibration of imaging data sets. The next section provides a broad overview.

4.0 SELF-CALIBRATION

In their groundbreaking paper in 2000, Arendt, Fixsen, and Moseley (AFM00) present a detailed investigation into how one might dither a data-set in an optimal way to allow the best possible self-calibration. Their effort was focused on coming up with the best possible dithering strategy for Spitzer, but much of their reasoning is independent of the particular instrument at hand. In this section, we will give a brief summary of their results. Much of the background in this section comes indirectly from AFM00.

4.1 What is self-calibration?

It is helpful to think of L-flat mitigation as a “passive” correction for calibration errors, and self-calibration as an “active” correction. Self-calibration means using the same data that were taken for science to extract information about the detector itself, which in turn can be used to improve the scientific product. Typically, the science data are taken with a variety of offsets, so that a given pixel will sample different parts of the scene in different exposures. The flux recorded by an observed pixel can be thought of as being mostly due to the counts it received from the source, but the pixel value also reflects the bias and gain of that particular pixel:

$$\mathbf{P}[i,j] = \mathbf{B}[i,j] + \mathbf{G}[i,j]*\mathbf{S}[i,j], \qquad \text{[Eqn. 1]}$$

where, **P** is the pixel array, **B** the bias, **G** the gain, and **S** the intrinsic flux received by the pixel (the scene, which we would like to recover). The bold font here, and for the rest of the report, indicates an image array; we will usually suppress the indices below.

In general, standard pipeline reductions use a super-bias frame for **B** and a flat-field reference file for **G**. The bias frame **B** comes from a large number of calibration observations taken at around the same epoch, possibly with adjustments to incorporate the reference-pixel data taken along with the science exposure itself. The flat-field reference frame **G** is constructed for each filter, with the high-frequency component coming from ground-based or in-orbit lamp-flats and the low-frequency, "L-flat" component constrained by observations of a standard calibration field.

There are several reasons why the pipeline reference files for either **B** or **G** (or both) might be less than optimal for a given data set. For example, if the bias image varies over time, then the epoch used to construct the bias reference files may not be sufficiently local, or the local frames available may not provide sufficient S/N to generate an accurate bias frame. This might be the case if the spatial structure in the bias is sensitive to the details of the thermal state of the telescope. Also, the gain frame **G** can also suffer from transient issues that would make the pipeline reference file inadequate. For instance, variations in vignetting or differences between how a flat-field lamp and the sky illuminate pixels can cause the pipeline reference **G** to diverge from the flat-field that is ideal for a given dataset.

If there is reason to distrust either **B** or **G** (or both), and if the science data are taken judiciously, then it is possible to solve for them along with the scientific scene. One of the main drivers of all dithering by more than fractional pixels has always been the acknowledgement that there can be errors in **B** and/or **G**, and by placing the same part of the scene in different pixels, we will naturally average out these errors. Such "flat-field-error mitigation" can be accomplished without undertaking an explicit self-calibration. Self-calibration takes this mitigation a step further. Not only are we attempting to average out detector-related errors, but we are aiming to remove them. It turns a "passive" correction into an "active" correction.

The self-calibration idea is that if each exposure is a realization of the same astronomical scene, parametrized by reference-frame coordinates (I,J), then we can replace **S**[j,j] above with $\mathbf{F}[I+\Delta I_n, J+\Delta J_n]$, where **F**[I,J] is the scientific scene in the reference frame, which is constant from exposure to exposure, and where $(\Delta I_n, \Delta J_n)$ represents the dither that maps the reference frame into an individual frame n: $(i_n, j_n) = (I+\Delta I_n, J+\Delta J_n)$. It is easiest to deal with only full-pixels dithers, but some accommodation can be made if the dithers include fractional pixels. (This is mentioned briefly in AFM00, but is not addressed explicitly. At any rate, undersampling should only be relevant for MIRI's shortest wavelengths.)

If we have N sets of exposures and know the dither offsets between them, then we have $N \times N_I \times N_J$ equations like Eqn 1 above, where N_I and N_J represent the dimensions of the image. If we want to solve for **B**, **G**, and **F**, then we have $3 \times N_I \times N_J$ unknowns, and a formal solution is possible for $N \geq 3$ exposures. Unfortunately, there are many degeneracies involved in this solution, so it is in general not sufficient to simply have more equations than unknowns. The nature of the scene and the quality of the dithers will have a large impact on the quality of the solution.

4.2 Dependence on the nature of the scene

Our ability to solve for **B** and **G** separately depends on the nature of the scene we have to work with. If the scene has a large dynamic range with a good distribution of pixel values across its (I,J) domain, then it is possible to solve for both **B** and **G** independently, since a low pixel value will measure **B** better, and a high pixel value will provide a better constraint on **G**.

On the other hand, if the scene is flat, with **S**[I,J] having pretty much the same value everywhere across its domain, then we cannot solve separately for **B** and **G**, as changing **B** by 1 is degenerate with changing **G** by 1/**S**. In the case where we happen to know one of the reference images better than the other, it is then possible to solve for the other even with a predominantly flat scene. In fact, it is often the case that one of either **B** or **G** is better known, so having a flat scene is not always a liability since we need to solve for only one of the two. This is the general case that AFM00 were focused on.

4.3 Dependence on the dither pattern

Our ability to measure **B**, **G**, and **F** independently is equally dependent on the dither pattern. If there is no dither pattern, then we cannot measure **B** and **G** independently from **F**. The main focus of Arendt, Fixsen, and Moseley (2000) is to understand how the choice of dither pattern can impact the quality of a self-calibration. They concentrate on the regime where one can assume to know either **B** or **G**, and we simply want to solve for one or the other of them, along with the scene **F**. For simplicity, we will solve here for **G**, though the same argumentation goes for **B**.

Let us assume that we have N dithers of $(\Delta I_n, \Delta J_n)$. A particular part of the scene with a flux $F = \mathbf{F}_{IJ}$ will land in pixels $(i_n,j_n) = (I+\Delta I_n, J+\Delta J_n)$ in the different exposures, so that:

$$\mathbf{P}_{in,jn} = \mathbf{B}_{in,jn} + \mathbf{F}_{IJ} * \mathbf{G}_{in,jn} ,$$

or,

$$\mathbf{G}_{in,jn} = \mathbf{P'}_{in,jn} / F,$$

where $\mathbf{P'} = \mathbf{P} - \mathbf{B}$. The above gives us N equations relating $G_{in,jn}$, $P'_{in,jn}$, and F. If we eliminate F from all the equations, then we can obtain relations between the G-values for the various pixels that this location of the scene is dithered into: $G_{i1j1} = G_{i12j2}*(P'_{i1j1}/P'_{i2j2}) = G_{i13j3}*(P'_{i1j1}/P'_{i3j3})$, etc. The equations also give many estimates of the scene: $F \sim \Sigma\, P_{ij}/G_{ij}$. The more independent pixels the scene is dithered into, the more constraints

we have on the scene itself, and the more independent inter-relations we have among the pixels that sample the flat fields.

4.4 The findings of AFM00

AFM00 demonstrate that the best constraints on the **G** array will come from maximizing the number of independent inter-relations we have among the elements in **G**. This flows directly from the number of independent dither baselines we have available.

As an example, if we have four dithers with offsets of (0,0), (5,5), and (10,0) (15,5), then scene pixel A at (50,50) in the reference frame will land in pixels (50,50), (55,55), (60,50) and (65,55), giving us inter-relations among these four pixels in the **G** array, as seen in the previous section. If we now consider scene pixel B at (60,50) in the scene, then we will get relations between G[60,50], G[65,55], G[70,55] and G[75,55]. Because the dither offset between dither #1 and dither #2 is the same as that between #3 and #4, both of these sets of inter-related pixels contain G[60,50] and G[65,65], and as such we get fewer independent constraints on **G**, and thus will incur more redundancy in our solution for them than we otherwise would.

The need for non-redundant baselines is related to the fact that the self-calibration solution for **G** is essentially an effort to establish the value of each pixel in **G** relative to every other pixel in **G**. Since it would require $N_I \times N_J$ dithers to allow a direct comparison between every pixel pair, most pixels are inter-compared using intermediaries: pixels 1 and 2 are compared, and pixels 2 and 3 are compared, allowing some linkage between pixels1 and 3. The quality of this linkage depends on how many "degrees of separation" there are between typical pixels. The best solutions clearly result when there are fewer intermediate steps.

The main thrust of AFM00, then, is to underline how important it is to execute as many independent dither baselines as possible. They investigated several varieties of dither patterns in an effort to determine which had the largest number of independent baselines, and assigned a "figure of merit" (FOM) to a variety of patterns in order to assess how much redundancy a given pattern has. This FOM is an indirect measure of the number of independent baselines and comes from the off-axis covariance-matrix elements of the linear solution for **G** (or **B**). The FOM metric was evaluated for a variety of dither patterns: geometric patterns, various VLA set-ups, Reuleaux patterns, random patterns, Gaussian patterns, box patterns, and other specific patterns that have been used for particular datasets (such as the pattern used for the HDF with NICMOS and for the HUDF with ACS/WFC). They found that some strategies performed well in general, while others were clearly inferior. They also found that different strategies performed differently depending on how many dithers were required.

4.5 Remaining open issues

While AFM00 introduced and fleshed out a lot of important concepts in regards to dithering for self-calibration, there are a couple of issues relevant to JWST that are not

fully explored. We will discuss them below, and will elaborate on their relevance to JWST in §5.0.

4.5.1 Dithers and anticipated structure in G

One issue that AFM00 touches on, but does not fold directly into their figure-of-merit calculations, involves the particular structure that is trying to be resolved via self-calibration of **G** (or **B**). If it is the pixel-to-pixel structure they are trying to constrain, then the treatment they prescribe, wherein no pair of scene pixels is dithered from the same detector pixels to the same detector pixels more than once, is indeed the most important consideration. However, if the unknown structure of interest in **G** is of a larger scale than a few pixels, then dithers that are independent in a single-pixel sense may not be independent in terms of adequately sampling the variations of interest in **G**. In this case, the dither baselines would need to probe the relevant scale of **G** variations.

It is reasonable, in fact, to think that the pixel-to-pixel component of the flat fields might be well constrained by the lamp flats, and that it is the larger-scale variations that are more responsible for the structure in **G** or **B** that we are trying to resolve. This could be the case if there are thermal gradients across the telescope that may interplay with variations in vignetting, producing a varying bias or background across the detector. To the extent that the calibration reference files are constructed under different thermal conditions than the observations, self-calibration might result in an improvement in measurement of the science scene **S**.

The issue of probing structure in **G** is discussed in AFM00, but it is not discussed in the context of how far apart dithers must be to be truly independent as far as the structure is concerned, and it is not explicitly included in their more general FOM calculations. It should be possible to evaluate dithers in terms of resolving a particular anticipated power spectrum in **G**. Dither independence in this sense would be relevant. Without such a focus, it is hard to evaluate the quality of the various dither patterns.

It is worth noting that if the only focus is on pixel-to-pixel variations in **G**, then it is possible to develop a dithering strategy that has the smallest pattern possible without repeating any dither-to-dither baselines. Appendix A describes one such strategy. Once the target structure in **G** is larger than pixel-to-pixel, a closed-form optimal solution is harder to construct, as there are trade-offs between field coverage and which baselines are more important to probe.

4.5.2 Noise and the figure of merit

Another aspect of the self-calibration solution for **G** that is not discussed in AFM00 concerns noise in the observations. There will of course be some noise in the observed pixel array, **P**. This noise will naturally impact the precision with which we can measure the scene **S** and the flat-field **G**, but it can also have an impact on how redundant a given dither baseline is.

Consider the case where most of the pixels in the scene **S** are sky pixels, and the background is relatively low. Say, the background has 100 e^-, so that each background

pixel has a noise of about 10%. Now, if the **G** array from the pipeline is known to be constant to 5%, then we need to achieve at least this precision to justify the self-calibration. Given that each pixel provides only a ¼ -σ measurement of **G**, it matters little whether we compare G[10,10] to G[20,20] more than once, since each time we compare the two pixels we improve our constraints, so long as the noise is different in each measurement.

It is clear that the AFM00 analysis implicitly assumed a very bright sky background where most of the signal in the individual observations was due to real differences in **G** or **S**, and not due to noise. If the noise is larger than the pixel-to-pixel variation in **G**, then a little baseline redundancy is clearly less of an issue. Redundancy in this case can be thought of as the equivalent of taking twice or three times the exposure time for each observation.

4.5.3 What is being self-calibrated?

In the situation where we may know some aspects of **G** (say, its pixel-to-pixel structure) but not other aspects (such as its large-scale gradients), then rather than solving for the entire **G** array pixel-by-pixel, we may prefer to solve for $\boldsymbol{\delta G} = (\mathbf{G} - \mathbf{G_{ref}})$, the difference between the true flat field and the reference flat. This array could be parametrized in such a way as to focus on the structure of interest. The distribution of dither baselines will naturally have an impact on how well constrained $\boldsymbol{\delta G}$ will be; to constrain $\boldsymbol{\delta G}$, the baselines clearly must be large enough to probe its structure. It is also worth considering that if we are probing larger-scale structure in $\boldsymbol{\delta G}$, then the noise issues discussed above in §4.5.2, might become less relevant, as each independent element in $\boldsymbol{\delta G}$ will involve many pixels, and as such will provide a significant root-N improvement factor.

5.0 Applications to JWST

We noted in the introduction that the MIRI dither patterns have been constructed so that self-calibration would be possible, whereas the NIRCam patterns were not designed with self-calibration as an explicit option. Here we discuss these decisions in the context of the self-calibration discussion of §4.0.

5.1 MIRI

As we mentioned above in §3.2, the two primary MIRI dither patterns (the 12-point Reuleaux pattern and the 311-point Cycling pattern) were constructed with self-calibration explicitly in mind. As a result, the baselines between dithers provide a nice figure-of-merit, in terms of the Arendt, Fixsen, and Mosely (2000) metric.

Neglecting instrumental effects, the MIRI background is expected to be dominated by 5 components: thermal emission from the Zodiacal dust, scattered light from the Zodiacal dust, diffuse Galactic emission, and thermal emission from the telescope and starshade. We list the estimated backgrounds in each of the MIRI direct imaging filters in Table 1 using estimates for the telescope and instrument performance and for the telescope and

sunshade emission from G. Rieke's MIRI Sensitivity Calculator (MIRIradmodeldb.xls spreadsheet).

It is clear that there will be significant background flux for all of MIRI's filters. Some of the sources of these backgrounds (particularly the sunshield and telescope, which contribute mostly at longer wavelengths) may vary with time and, to the extent that their imprint on the detector is not uniform, we should be pro-active in ensuring that data sets that may benefit from a self-calibration can be dithered in such a way as to make one possible.

The strategy needed to address MIRI's backgrounds is wavelength dependent because the dominant source of the background is wavelength dependent. The background at shorter wavelengths (< 13 μm) will be dominated by sky backgrounds such as thermal emission from Zodiacal dust that are not expected to change during an observatory visit. These observations will also suffer from mild under-sampling, suggesting that the offsets in the primary patterns should be relatively small at short wavelengths (so that the dithers can maintain their pixel-phase coherence). By contrast, the background in longer wavelength observations will be dominated by scattered light and thermal emission from the telescope and sunshade that are expected to change during an observatory visit. Since

Table 1 MIRI Backgrounds

Filter	Thermal Zodiacal	Scattered Zodiacal	Thermal Telescope	Thermal Sunshade	Total
	(γ s^{-1} pix^{-1})	(γ s^{-1} pix^{-1})	(γ s^{-1} pix^{-1})	(γ s^{-1} pix^{-1})	(γ s^{-1} pix^{-1})
F560W	5.0	0.1	0	0.6	5.7
F770W	33	0.1	0	6	39
F1000W	53	0	0	13	66
F1130W	24	0	0	20	44
F1280W	79	0	0.8	100	180
F1500W	120	0	26	320	470
F1800W	84	0	240	390	710
F2100W	96	0	1600	820	2500
F2550W	58	0	7100	1000	8200

changes in facility background are expected to create low frequency structure in the background emission and since the observations are well-sampled, the offsets in the patterns should be larger at longer wavelengths. For these reasons, Chen 2009 created a mapping between filter wavelength and pattern size (small, medium, or larger) that will be executed by default unless an observer specifies other needs (e.g. equal sky coverage in every filter).

The investigation in AFM00 was undertaken largely in anticipation that individual Spitzer programs might benefit from self-calibration, and the Spitzer dither patterns were optimized with this in mind. It turned out (Casertano, personal communication) that the Spitzer calibration was much more stable than anticipated, and thus that the self-calibration aspects of the dither patterns were not generally utilized. Nevertheless, even though Spitzer did not need to make use of the self-calibration capabilities of the dither patterns, the fact that the patterns were optimized with this in mind did not end up compromising any of the science. The self-calibrating patterns still accomplished the defect-avoidance and L-flat mitigation that any dither pattern would accomplish, and did not unnecessarily spread out the field, so nothing was lost by enabling self-calibration. The same is the case for the MIRI patterns. It may not in the end be necessary to do self-calibration (for example if the thermal backgrounds are more stable than in today's worst-case scenarios). But it will be good to have that option built-in, just in case, particularly as the dither patterns that are optimized for self-calibration also accomplish all the other goals of dithering.

5.2 NIRCam

The primary patterns for NIRCam were developed by Anderson (2009) and are discussed in §3.1 above. The main goal of these patterns was to mitigate the effects of the inter-chip and inter-module gaps, in order to ensure that the coverage of a field will be as even as possible. A second aim of the patterns was to ensure that a given object not fall on the same pixels more than once, which helps to mitigate the impact of flat-field errors and detector defects. This second goal is met as a natural byproduct of the large dithers needed to accomplish the first goal (gap coverage).

The NIRCam patterns were not optimized for self-calibration, and it turns out that the patterns have a low figure-of-merit in the AFM00 metric. This is because they are made up of baselines that repeat. For instance, in order to deal with both the module gap and the SCA gaps (see Figure 1), it is necessary to dither within a tight range centered on $\Delta x = 58''$. Three dithers do a nice job covering almost every point in the field in at least two out of three pointings (68% is the theoretical maximum). When the dither patterns are generalized to 6, 9, 15, 21, 27, 36, and 45 points, the larger patterns are made up of these gap-optimized 3-point patterns — to do otherwise would compromise the evenness of the field coverage. The downside of repeating the same small pattern is that we end up with many redundant baselines, resulting in a low figure-of merit in the AFM00 metric.

When considering the dithers for the 45-point pattern specified in Table 4 of Anderson (2009), we find that only 152 out of the 990 (N*(N−1)/2) dither baselines are completely independent (considering the 2-d vector offsets). 206 of them repeat twice, 66 repeat three times, 196 repeat 4 times, etc. From this perspective, the NIRCam pattern would appear to have serious problems for use in self-calibration[1].

[1] In this heuristic analysis, we only consider the first level of neighbors, and do not consider neighbors' neighbors. Nonetheless, it is clear that repeated dither baselines will only harm the AFM00 FOM.

There are several reasons this poor FOM should not be a concern. First, the background in NIRCam is expected to be quite low, so that the background pixels will have very low S/N and therefore a very fuzzy handle on constraining the flat-field or bias. As a result, it is not as redundant to compare the same two pixels more than once to improve **G** or **B**, since each additional comparison will improve the constraint. Second, the offsets specified in the table are in arcseconds, not pixels, for the simple reason that distortion will cause a dither in one location to have a different pixel span than in another location. The result of this will be that the "same" baselines discussed above will not in fact map the same set of pixels into the same corresponding set of pixels. As a consequence, the pixel-to-pixel aspect of the AFP00 figure-of-merit metric will still be extremely high. However, if the goal is to solve for arcsecond-scale structure in **G**, then the dither baselines will once again provide redundant information.

It is not clear what scales (if any) we will need to concern ourselves with for variation of NIRCam's bias or flat-fields. NIRCam is almost completely insensitive to thermal variations in the mirror or sunshield, so those issues will not come into play. The only time-sensitive issue that could come up concerns variations in vignetting as the primary mirrors are adjusted. Such variations in vignetting presumably would affect only the outer edges of the field, so that any self-calibration would involve a more limited domain, a domain, which was not explored in AFM00.

We conclude that the NIRCam patterns were properly designed to deal with the largest, and best known, challenge: mitigating the gaps between the chips and modules. While the pattern that optimizes the even-ness of the coverage is not optimal for self-calibration, given the expected low-signal in the background, a moderate amount of redundancy in the dither baselines should not degrade a self-calibration solution, in the unlikely case that one should prove useful.

6.0 Results from simulations

The general necessity of self-calibration for JWST was investigated by Casertano and Holfelz (2002). They consider the science case for self-calibration in NIRCam and MIRI, without focusing on specific dither patterns. They use simulations of galaxy-filled fields to investigate how flat-fielding errors impact science, and how the science images can be used to improve the flat fields, thereby improving the science in a virtuous cycle.

They find that the low background of NIRCam makes the search for faint objects photon and read-noise limited. As a result, errors in the flat-field correction (which tend to be about 1%) will have very little impact on this important science driver. This is fortunate, since the low background makes it extremely difficult to do an accurate self-calibration, given the low signal-to-noise in each sky pixel.

They found that MIRI, on the other hand, will be background-limited at almost all wavelengths, and as a result MIRI's flat-field correction needs to be much better in order to match the photon noise of the background. To reliably find faint objects on the high background, MIRI's flat fields will need precisions approaching 1 part in 10^4. Dithering can mitigate this requirement somewhat by $\sqrt{N_{dith}}$, and the fact that each source falls on several pixels also helps, but it is clear that science will benefit greatly from the best

possible calibration files. Casertano and Holfelz conclude that self-calibration might indeed be a useful option for large MIRI programs.

The report compares the efficacy of constructing improved flat fields from either sky flats spanning multiple programs, or from self-calibration within a single large dithered set. They find that both efforts can produce flat fields of sufficient quality for JWST's science requirements, but the super-sky-flat approach must assume that the flat-field is constant across several observing programs.

In a follow-up effort, Holfelz and Casertano (2003) investigate how competitive a super-sky-flat approach is compared to the formal least-squares self-calibration approach when both are restricted to the same well-dithered observing program. Not surprisingly, they found that the self-calibration approach resulted in a calibration that was better by about 20%, since this approach makes use of all the pixels, not just the pixels that are determined to be part of the background. However, both approaches produced flat-fields that were of sufficient quality for high-precision science.

The focus of their studies was not on the impact of particular dither patterns, but rather on the post-observation analysis, under the presumption that a good pattern was used. They investigated spiral patterns, with a small random component, and a purely random pattern with offsets of a fraction of the detector, and their results were not very different for the two approaches, but this aspect of the investigation was not exhaustive.

7.0 Conclusions

We have considered the demands and benefits of a self-calibration-focused strategy for dithering. Both MIRI's and NIRCam's strategies will allow for some level of self-calibration, but only MIRI's strategy is explicitly optimized to allow self-calibration of the bias and/or the flat-field/gain arrays.

Most MIRI images will have a high background, so it is in a unique position to make use of a self-calibration strategy. The high background means that comparing one pixel to another will give an accurate measurement of the relative flat fields, thus providing the high-precision constraints that make self-calibration possible. The high background also makes MIRI more dependent on good flat-fields for faint-source identification, so it is fortunate that such a precise calibration is in principle feasible.

In addition, much of MIRI's background may have a component that depends on the thermal state of the telescope and sunshield, so it is natural that MIRI would want its dither pattern to enable some kind of self-calibration to construct the mostly timely calibration possible. Whether self-calibration is useful in practice will depend on how stable the telescope turns out to be in practice. If the observatory is stable enough to allow super-sky flats to be more accurate than self-calibrated flats, then self-calibration will not be necessary. This was found to be the case for Spitzer. However, we do not yet know how stable the observatory will be, so it is safer to optimize MIRI's dither patterns to enable self-calibration. Since the MIRI FOV does not have gaps to consider in its dithering strategy, it costs little to space out the dithers to get a good self-calibration figure-of-merit.

NIRCam's dithering strategy was optimized to ensure that spatial coverage would be as even as possible in the presence of inter-chip and inter-module gaps. It turns out that this dithering strategy is inherently incompatible with a self-calibration-focused strategy. This can be seen simply in that imaging over the gaps requires repetition of specific dither offsets, and using multiple dithers of the same spacing introduce costly redundancies in the self-calibration solution. Given the anticipated low level of the background in NIRCam, a high-precision self-calibration would be difficult from a signal-to-noise perspective, even with an optimized dither strategy. Thus, the redundant dithering baselines are not really a serious limitation. Fortunately, the science drivers for NIRCam should not require better than 1% errors in the flat fields, so self-calibration should not be necessary.

8.0 References

Anderson, Jay. 2009 JWST-1738. Dither Patterns for NIRCam Imaging

Arendt, Richard G., Fixsen, D. J., & Moseley, Harvey. 2000 ApJ 536 500-512, Dither Strategies for Efficient Self-Calibration of Imaging Arrays

Carey, S., Surace, J., Glaccum, W., Lowrance, P., Lacy, M. & Reach, W. 2010, IRAC Data Handbook

Chen, Christine H. 2009 JWST-STScI-001657. MIRI Imaging Dither Patterns

Holfelz, Sherie & Casertano, Stefano. 2003, STScI-JWST-R-2003-0002, Further Comparisons of Super-Sky and Self-Calibration Flat fields for Simulated Mid-Infared JWST Images

Casertano, Stefano & Holfelz, Sherie 2002, STScI-JWST-R-2002-0004, Comparison of Super-Sky and Self-Calibration Flat Fields for Simulated Mid-Infrared JWST Images

Appendix A

If the only consideration is maximizing the number of independent dithers, and minimizing the overall span of the dithers, then it should be possible to solve this problem in closed form. We can choose a set of N dithers that (1) have *no* repeating baselines and (2) span the smallest region possible.

We generated a simple computer program to come up with such an optimal dither pattern for up to 50 dithers. The integer-pixel dithers reported in Table 2 all have independent baselines, in the sense that $(X_m - X_n,\ Y_m - Y_n)$ is different for all choices of m and n. Figure 1 shows the dithers and the array of 50*(50−1) = 2450 independent baselines.

Table 2: The fifty tightest unique dither baselines.

Dither Index and X and Y offset														
1	0	0	**11**	9	0	**21**	7	19	**31**	2	38	**41**	36	38
2	0	1	**12**	6	7	**22**	1	25	**32**	38	4	**42**	2	53
3	1	0	**13**	0	11	**23**	23	10	**33**	37	11	**43**	47	29
4	1	2	**14**	5	12	**24**	8	24	**34**	12	39	**44**	28	49
5	3	0	**15**	13	7	**25**	28	8	**35**	39	19	**45**	57	1
6	0	4	**16**	16	4	**26**	18	23	**36**	34	29	**46**	20	56
7	4	3	**17**	0	17	**27**	30	0	**37**	3	45	**47**	60	11
8	2	6	**18**	11	16	**28**	6	31	**38**	16	43	**48**	16	62
9	6	2	**19**	16	12	**29**	25	20	**39**	47	1	**49**	2	65
10	8	3	**20**	20	2	**30**	15	33	**40**	49	14	**50**	56	34

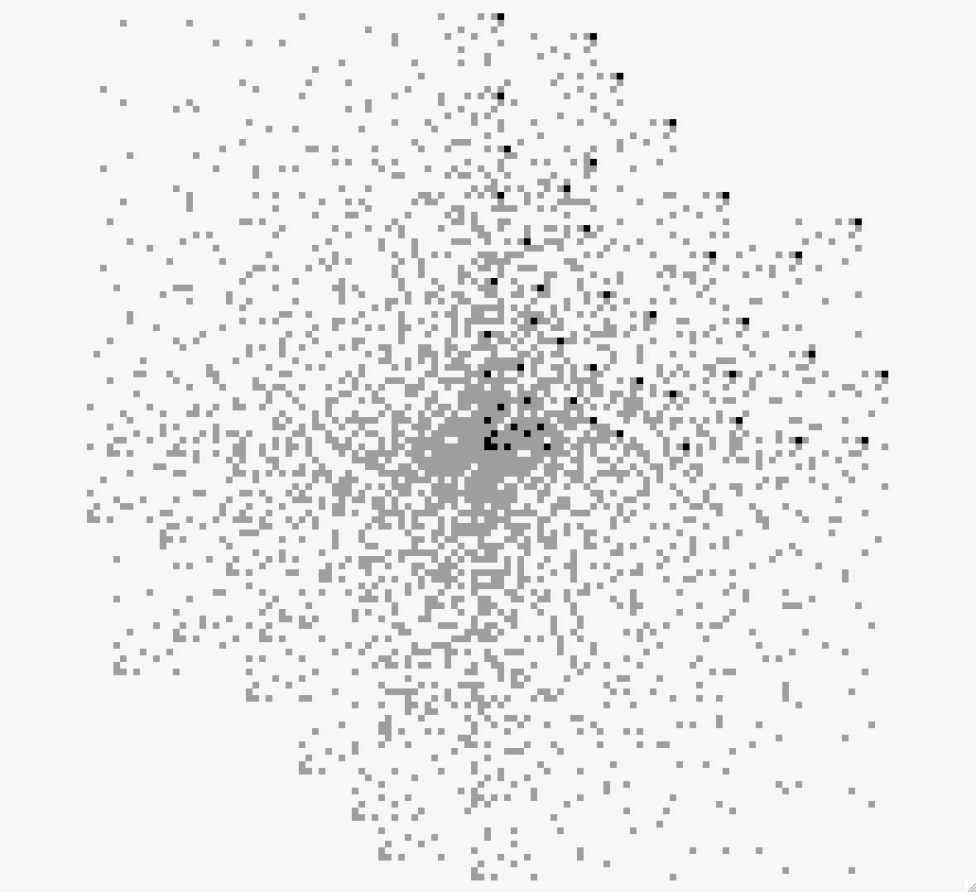

Figure 2: Dark points: the 50 dither offsets from Table 1. Light points: the 2450 independent baselines that can be constructed with these dithers.

If the only goal in dithering is to solve for the pixel-to-pixel component of **G** (or **B**), then such a dither pattern would be ideal. Of course, one might also want to probe only baselines longer than 5 pixels or so, to ensure that each source will land in independent pixels, but removing the first couple of dithers would solve that problem.